Interference with positive parity states is observed throughout the region investigated, and the finite value of A_3 strongly indicates that this interference is mainly $E1$-$E2$. The particle-hole model is used to extract an $E2$ cross section from the data, and the strength and nature of this cross section is suggestive of a quadrupole giant resonance. The 1p-1h model using harmonic-oscillator wave functions is unable to give the correct sign to the asymmetry coefficients A_1 and A_3, and it is concluded that 2p-2h excitations should be included.

ACKNOWLEDGMENTS

The authors wish to thank G. Holland and the synchrotron operators R. Pritchard, J. Sayre, and L. Severeide for their skill and assistance in the data acquisition. We acknowledge with thanks the painstaking efforts of H. Austreheim in constructing the fragile gas-target cell. Valuable discussions were held with Dr. B. Cooper, and we thank Dr. B. C. Cook for assistance in running the data through his least-structure computer routine.

PHYSICAL REVIEW VOLUME 186, NUMBER 4 20 OCTOBER 1969

Study of $Be^9(Li^7, p)$, $Be^9(Li^7, d)$, $Be^9(Li^7, t)$, and $Be^9(Li^7, \alpha)$ Reactions from 5.6 to 6.2 MeV†

F. D. SNYDER AND M. A. WAGGONER

Department of Physics and Astronomy, The University of Iowa, Iowa City, Iowa 52240

(Received 18 April 1969)

Absolute differential cross sections at angles ranging from 10° to 170° and at bombarding energies of 5.6, 5.8, 6.0, and 6.2 MeV have been measured for the reaction Be^9+Li^7, leading to each of the following states: ground and 0.75-MeV states of C^{15}; ground, 6.10, 6.58 with 6.72, 6.89 with 7.01, 7.34, and 8.32-MeV states of C^{14}; ground, 3.09, and 3.68 with 3.85-MeV states of C^{13}; ground, 0.95, 1.64, and 2.62 with 2.72-MeV states of B^{12}. The yields of the α_0 and α_2 groups at 20° (lab) have been measured at 3.3 MeV and at eleven other energies ranging from 5.0 to 6.2 MeV. Absolute cross sections were obtained by comparison of the yields of reaction products to elastic Coulomb scattering. Comparison is made of the total cross-section values with the $(2J+1)$ rule. The angular distributions for the t_0 and t_1 groups, at each of the bombarding energies, are compared with the predictions of a two-mode (pickup and heavy-particle stripping) direct-reaction process in the plane-wave approximation.

I. INTRODUCTION

THIS paper reports the results of an investigation of the reaction Be^9+Li^7 at Li^7 bombarding energies of 5.6, 5.8, 6.0, and 6.2 MeV. Relatively little previous work had been done on this reaction. The proton groups associated with the first two states of C^{15} had been observed[1]; four α-particle groups corresponding to the formation of B^{12} states up through the 2.62- and 2.72-MeV states had been observed, their angular distributions measured at low bombarding energies, 2MeV[2] and 3.3 to 3.75 MeV,[3] and a comparison of their cross sections with the Li^7 elastic Coulomb scattering cross section made in the latter energy range.[3]

Figure 1 summarizes the energy relations of the various reactions which are kinematically allowed.[4]

In the present work, angular distributions of proton, deuteron, triton, and α-particle groups beyond the continuum for each type have been obtained from 10° to 170° at each of the four Li^7 bombarding energies noted. At each of the energies, all of the yields were obtained concurrently, resulting in good values for the relative cross sections for each particle group. The yields of the α_0 and α_2 groups at 20° (lab) were measured as functions of energy from 5.0 to 6.2 MeV and at 3.3 MeV. At 3.3 MeV the yields were compared to that of the elastically scattered Li^7 in order to obtain absolute cross sections.

II. EXPERIMENTAL METHODS

The singly ionized Li^7 beam used in this study was obtained from the University of Iowa's Model CN 5.5-MeV Van de Graaff, made by the High Voltage Engineering Corporation. The Li^7 filament source has been previously described.[5] The analyzed beam is regulated and calibrated to 0.3% or ±15.0 keV at 5 MeV.

† Research supported in part by the National Science Foundation.

[1] E. Norbeck, Phys. Rev. **105**, 204 (1957).

[2] E. Norbeck and C. S. Littlejohn, Phys. Rev. **108**, 754 (1957).

[3] R. K. Hobbie, C. W. Lewis, and J. M. Blair, Phys. Rev. **124**, 1506 (1961).

[4] T. Lauritsen and F. Ajzenberg-Selove (to be published). Only the material on $A=11$ and 12 is published (see Ref. 11).

[5] E. Norbeck, Phys. Rev. **105**, 204 (1957).

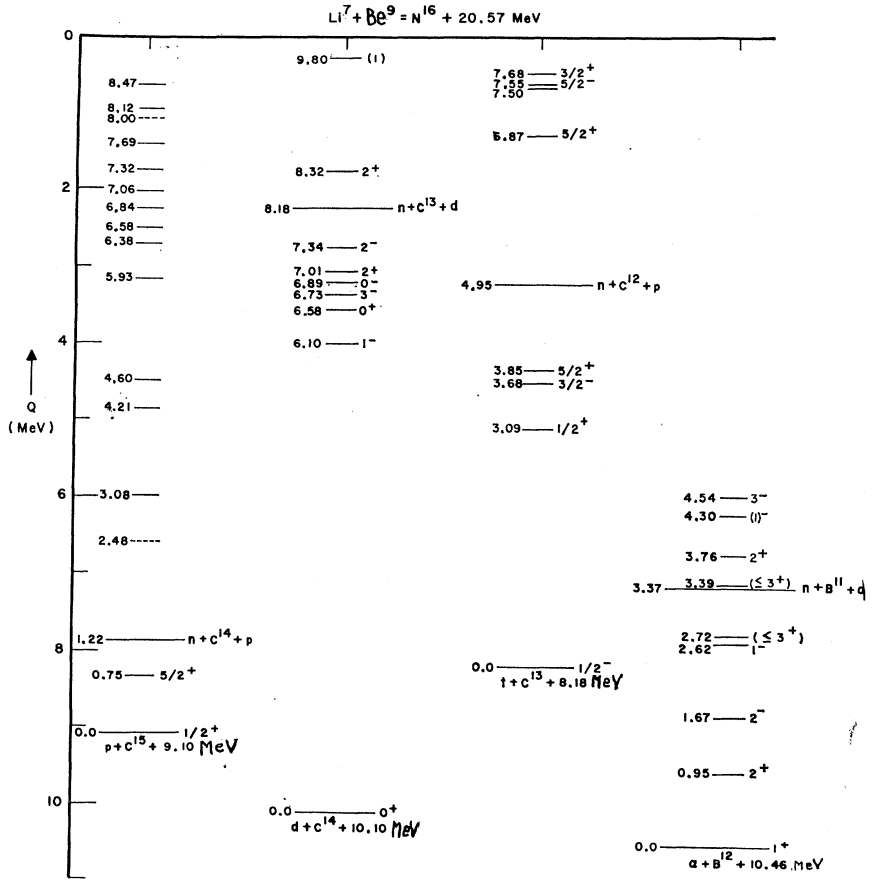

FIG. 1. Energy-level schematic for the relevant final states.

The target chamber used was a 17-in., model 600 scattering chamber made by Ortec. Figure 2 shows the basic beam-target-detector configuration employed. The top and bottom plates of the chamber, on which the detector assembly and the Ni foils used to stop the elastically scattered Li^7 beam were mounted, enable the detector and foils to be rotated in the reaction plane about an axis through the target. A monitor detector was mounted on the wall of the chamber at 20° from the beam direction and in the reaction plane. Sufficient foil was placed in front of this detector to stop the scattered Li^7 beam. Two pairs of collimators within the beam tube were used to define a beam spot on the target less than 2.0 mm in diameter.

The targets used in the angular distribution measurements were prepared by evaporating Be on 1.7-mg/cm^2 Al backing. These targets were about 100 keV thick to a 6.0 MeV Li^7 beam. The target used for the yield-curve measurement was prepared similarly, but was about 50 keV thick. The target used for the elastic scattering cross-section measurement was prepared by evaporating approximately 5-μg/cm^2 Be on teepol-coated slides. The target was then floated off and picked up in such a way that it doubled over the target holder, giving a final thickness of 10 μg/cm^2. This double thickness of the target material was easier to obtain than a single thickness and had the necessary strength.

Figure 3 is a schematic diagram of the detector and electronic arrangement. Conventional electronics and an on-line computer were used to gather, store, and analyze the data.

The monitor detector was collimated to 2.03×10^{-3} sr for a point source at the center of the chamber. Its depletion depth of 300 μ was sufficient to stop all the α particles from the reaction, but transmitted the charge-one particles with small energy loss. As a result, the charge-one particle peaks in the energy spectrum all appeared below the α peaks corresponding to the first four excited states of B^{12}. These α peaks could thus be easily used for monitoring purposes. (The Q value for the $Be^9(Li^7, He^3)B^{13}$ reaction is -5.2 MeV, so He^3 reaction particles were not observed in the present experiment.)

Particle detection and identification were accomplished by standard E, ΔE techniques. A stack of three totally depleted transmitting 50-mm^2 Si detectors were used in the E, ΔE detector assembly. The first detector was 40 μ thick and was used as the ΔE detector. The

two following detectors were each 1000 μ thick and were connected in parallel. The assembly was capable of stopping a 20-MeV proton. The maximum energy lost by a charge-one particle in the ΔE detector, and thus the minimum-energy α particle that could be separated from the charge-one particles, was about 2.5 MeV. The effective total angular aperture of the assembly was 1.51×10^{-3} sr.

Pairs of signals received by the ΔE and E analog-to-digital converters (ADC's), corresponding to the different types and energies of the reaction particles entering the E, ΔE detector assembly will lie along curves such as those shown in Fig. 4. The somewhat hyperbolic portion of each of the curves in the figure is a consequence of the energy lost in the ΔE detector by a charged particle of energy E passing through that detector varying approximately as $(E)(\Delta E)=$const. For each particle type there is an energy value for which all particles of that energy or less are completely stopped in the ΔE detector. This value is, of course, considerably higher for the α than for the charge-one particles. Since the ΔE signal is added to the $E-\Delta E$ signal to obtain the total E signal, as noted in Fig. 3, the resulting ΔE versus E dependence for a particle completely stopped in the ΔE detector is simply $\Delta E= E$. This gives rise to the straight-line portion of the curves in Fig. 4. It is important to note that when an α-particle signal lies along the straight line segment of the curve, it still contains particle identification information as long as ΔE lies above the value, marked ΔE_t in Fig. 4, corresponding to the maximum energy that a charge-one particle can lose in the ΔE detector. Thus, even though our ΔE detector completely stopped a 7-MeV α-particle, identification was possible down to about 2.5 MeV. At lower energies, data for all the particle types start to overlap one another and identification is lost.

The on-line computer was used to store the data from the E, ΔE system in a ΔE versus E matrix and the monitor data as a particle energy spectrum. These data were stored on tape and later recalled to separate the matrix into single-particle spectra and to sum the number of counts in each particle group. Representative single-particle energy spectra obtained in this way are shown in Figs. 5–8.

At a given bombarding energy and detector angle, the data for all types of reaction particles are obtained concurrently so that the yields of the various particle groups are in the correct ratio. The yields at one angle are normalized to those at another angle at the same bombarding energy by means of the monitor-detector data. The monitor detector was left at a fixed angle throughout the measurements required to obtain the angular distribution at a given energy. Variations in the yield of the α-particle groups in the monitor detector were therefore due to changes in the target thickness and integrated beam intensity over the duration of the runs, and their yield could be used to normalize the

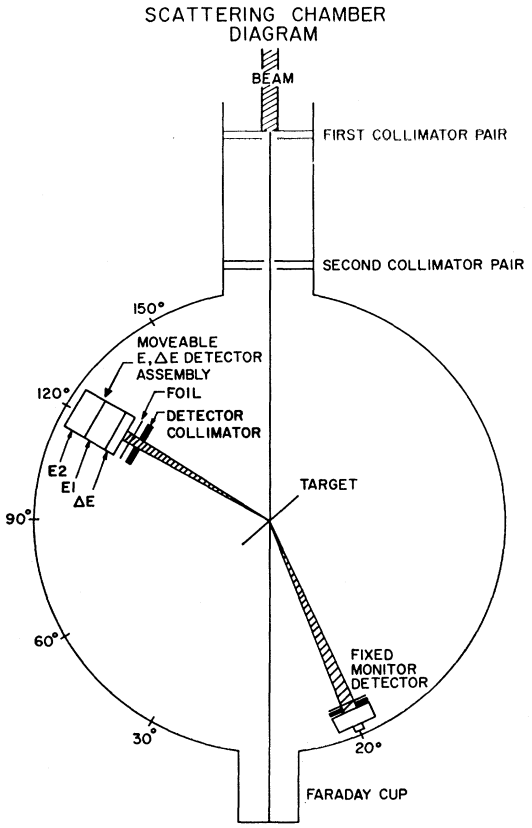

FIG. 2. Scattering chamber.

data for the different angles in the angular distribution at a given energy. The yield of the α_0 group which was cleanly resolved and free of contaminants at all bombarding energies was used for this purpose.

To normalize the yields of the various particle groups at one bombarding energy to those at another, the yields of the α_0 and α_2 groups were measured as functions of the bombarding energy for a measured amount of incident charge. (These groups are cleanly resolved and free of contaminants at the energies of interest and angle chosen.) The target was enclosed in a small cylindrical can within the scattering chamber and concentric with it. In the walls of the can were holes which let in the incident beam and permitted the reaction products to pass out at 20°. The can was used to guarantee complete charge collection, including secondaries produced at the target. The can and target, constituting the Faraday cup, were electrically connected but the pair insulated from the rest of the chamber. A grounded shield around the entrance hole prevented secondaries which might be produced at the last collimator in the beam tube from striking the can. This technique of obtaining a yield curve assumes that the target thickness is constant throughout the yield-curve measurement. To check for possible variation in

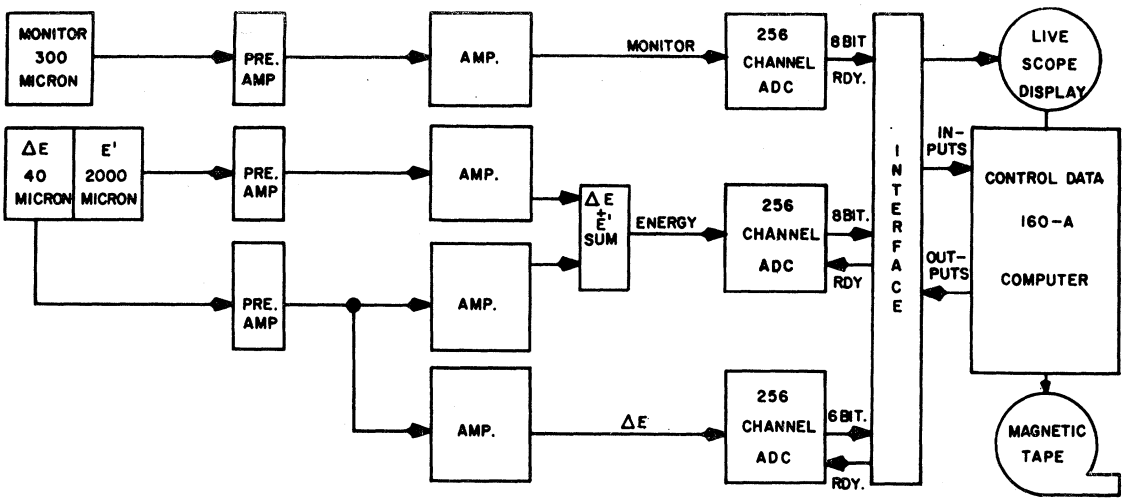

FIG. 3. Schematic of the data-acquisition system.

this thickness, various points on the yield curve were remeasured nonconsecutively as many as six times over the course of the measurements. The variations observed were within statistical uncertainty. The yields of the α_0 and α_2 groups from the yield curves were then compared to the yields of the α_0 and α_2 groups at the 20° points of the corresponding relative angular distributions. The ratio of these yields was used to normalize the angular distributions for different bombarding energies to one another.

To convert the relative cross sections for the various Be^9+Li^7 reactions studied in this work to absolute cross sections, an elastic scattering experiment was performed at a Li^7 bombarding energy of 3.3 MeV. For our purposes we wished to be able to assume that the cross section for the elastic scattering was the Coulomb scattering cross section. Thus we chose the low bombarding energy and an angle of 20°. At this angle and energy, the distance of closest approach of the Li^7 and Be^9 nuclei is about 20 F, and the sum of their radii is about 5 F. Hobbie *et al.*[3] have shown that the relative angular distribution for elastic scattering of Li^7 by Be^9 from 10° to 50° at a bombarding energy of 3.3 MeV is in agreement with the angular dependence of the Coulomb scattering cross section. We have proceeded, then, as if the cross section for the elastic scattering of Li^7 by Be^9 at 3.3 MeV and 20° were given by the Coulomb scattering cross section.

The absolute cross section for the $Be^9(Li^7, \alpha_0)B^{12}$ reaction was determined from the following relationship and indicated data:

$$\frac{d\sigma}{d\Omega}(E,\theta)\bigg|_{\text{c.m.}} = \frac{\text{yield } \alpha_0}{\text{yield Li}}\bigg|_{\text{lab}} \frac{G(\alpha_0)}{G(\text{Li})} \times \left(\frac{Z(\text{Li})Z(\text{Be})e^2}{E_{\text{c.m.}}}\right)^2 \frac{1}{16\sin^4(\frac{1}{2}\theta_{\text{c.m.}})},$$

where G represents the laboratory-to-c.m. system

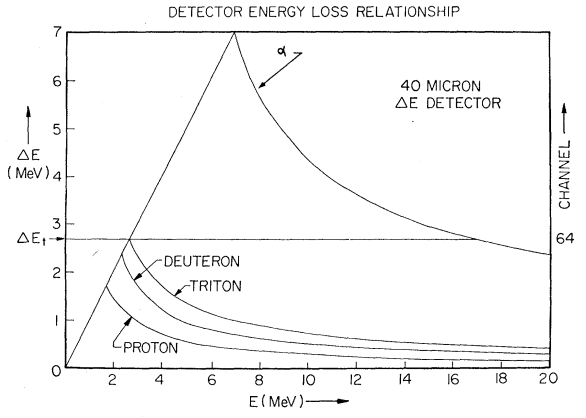

FIG. 4. $\Delta E(E)$ for the silicon detector.

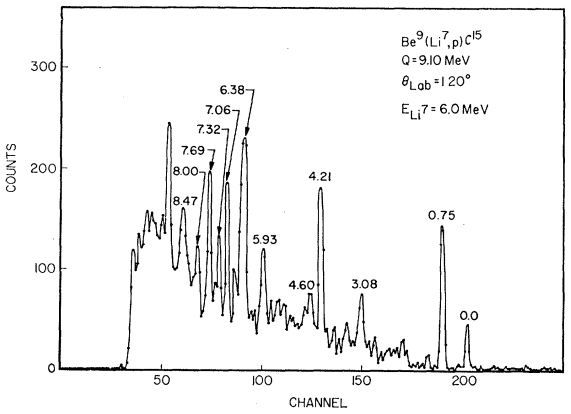

FIG. 5. Proton singles spectrum.

geometrical-conversion factor appropriate to the reaction indicated.

The circular collimator used on the detector in the measurements had a diameter of 3 mm, an angular diameter of 1.1°. The beam spot on the target was less than 2 mm in diameter, corresponding to an angular diameter at the detector location of less than 0.8°. Special care was taken in focusing the beam in all cases to make the beam intensity as uniform as possible over this beam spot. Because of the rapid variation of the Coulomb cross section with angle, the theoretical cross section was integrated across the face of the detector to find the effective cross section. The detector alignment was good to about ±0.1°, corresponding to a change of ±2% in the value of this integrated cross section. The statistical uncertainty in the yield of α_0 was 9%. The relative yields of the α_0 and elastically scattered Li^7 were measured concurrently. The detector was a high-

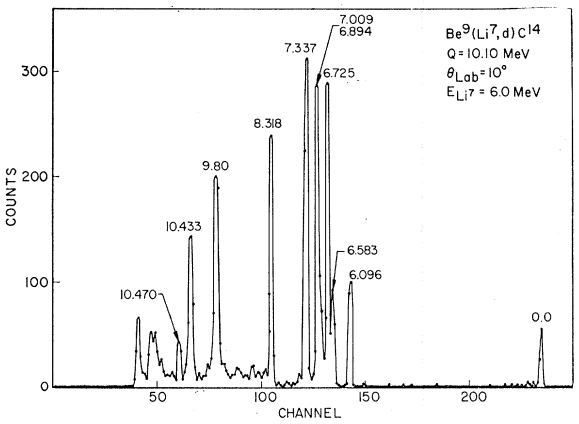

FIG. 6. Deuteron singles spectrum.

resolution 120-μ Si detector without absorbing foil. The singles energy spectrum obtained was stored in the computer with the Li^7 peak around channel 20 in a 1024-channel spectrum and the α_0 peak around channel 800. Figure 9 shows the spectrum obtained. Since the α_0 and Li^7 yields were measured concurrently by the same system, no separate monitoring system and normalization procedures were required and no correction had to be made for dead time of the system. (The counting rates of about 2000 counts/sec meant that dead time was not negligible. Since most of the events were stored around channel 20, the 4-MHz ADC used was adequate for the measurement.)

The absolute cross section obtained by the above method for the reaction $Be^9(Li^7, \alpha_0)$ at 3.3-MeV Li^7 bombarding energy and $\theta_{lab}=20°$ and the α_0 yield curve were then used to convert all the relative differential cross sections at higher energies to absolute cross sections. It is these that are shown in all figures involving cross section values.

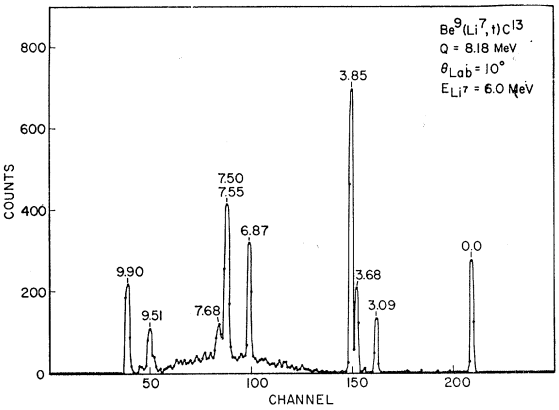

FIG. 7. Triton singles spectrum.

It should be noted that the value of 51±6 μb/sr which we have obtained for the absolute differential cross section for α_0 at 20° and 3.3 MeV is 30% lower than the value of 77 μb/sr obtained by Hobbie *et al.*[3] In both cases the value is based upon a comparison of the yields of α_0 and the elastically scattered Li^7. However, Hobbie *et al.* measured the $Be^9(Li^7, Li^7)Be^9$ yield and the $Be^9(Li^7, \alpha_0)B^{12}_{0.0}$ yield in separate experiments, whereas we have measured them concurrently. This procedure has enabled us to eliminate problems arising from unknown or varying target thickness, variation in beam intensity over the target spot, differences in detector geometry, and dead-time corrections. Further, the target used in the measurement by Hobbie *et al.* yielded enough $C^{12}(Li^7, Li^7)C^{12}$ scattering to make the Be^9 scattering data difficult to analyze. We have been fortunate in being able to make a target containing very little carbon, and have had the advantage of the better-resolution detectors now available so that the carbon scattering was no serious problem. Some of the problems of the earlier measurement have thus been eliminated

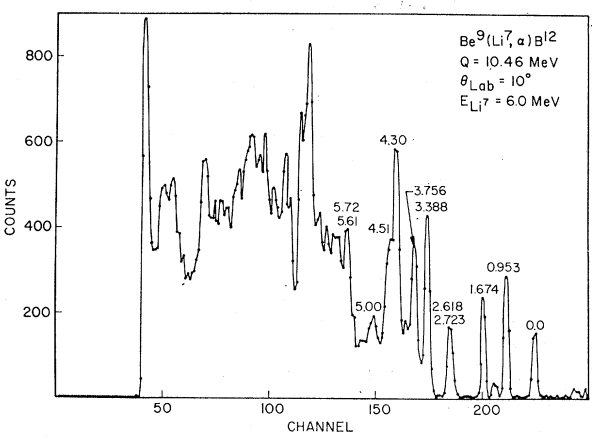

FIG. 8. α-particle singles spectrum.

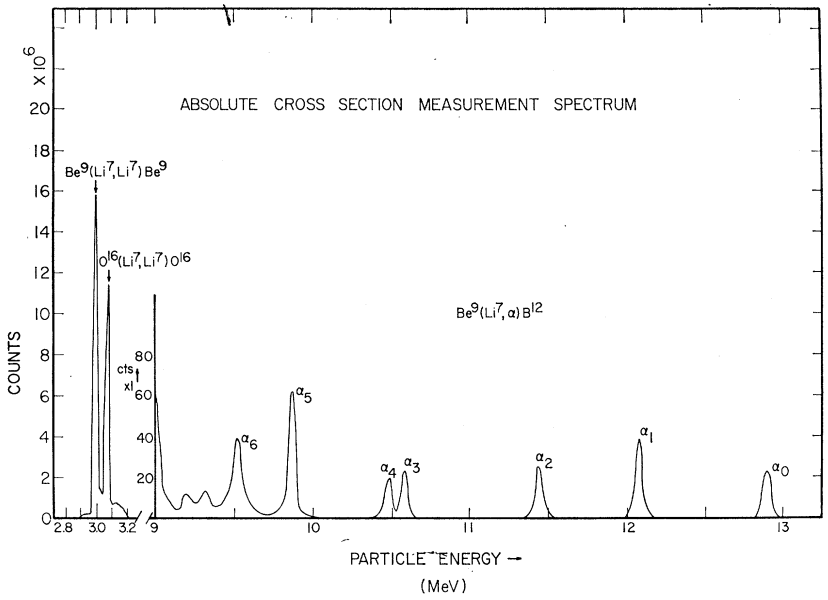

FIG. 9. Singles spectrum from the absolute cross-section measurement.

in the one we are reporting here. The present measurement was carried out twice at widely separated times (so anything peculiar about machine focusing, etc., should not be common to the two measurements), with different beam intensities and different targets. The cross-section values obtained in the two measurements agreed to within 6%, i.e., to within less than the statistical uncertainty in the yield of α_0.

III. RESULTS

Representative single-particle energy spectra are shown in Figs. 5–8. The yield curves for the α_0 group and for the α_2 group at 20° (lab) are shown in Fig. 10, and were obtained with an angular aperture of 1.606×10^{-3} sr.

The differential cross sections, obtained with a similar detector aperture, are shown in Figs. 11–18. The curves in these figures are simply smooth curves through the data points and do not represent the results of any detailed fitting procedure. The error bars shown on the angular distributions do not include the errors in the interenergy normalization. They reflect only the errors in the relative cross sections for a particular angular distribution. The error attached to an individual point is signified as a plain straight line if the main contribution is statistical deviation due to the finite number of events studied. Errors in points in which monitor error is significant are indicated with error bars capped with arrows. At points where contaminant was a problem, the error bars are capped with curves. The contaminants identified were: H^1, C^{12}, and O^{16}. The length of each type of error bar signifies one standard deviation on each side of the point.

An attempt was made to obtain angular distributions for some proton groups associated with the formation of higher excited states of C^{15}, in particular, p_4, p_6, p_{10}, p_{13}, and p_{14} associated with the formation of the 4.21-, 5.93-, 7.06-, 8.00-, and 8.12-MeV states of C^{15}. However, the errors involved in the subtraction of the continuum and contaminant background under these groups was comparable to the yield of the groups themselves and the analysis was not pursued further. The

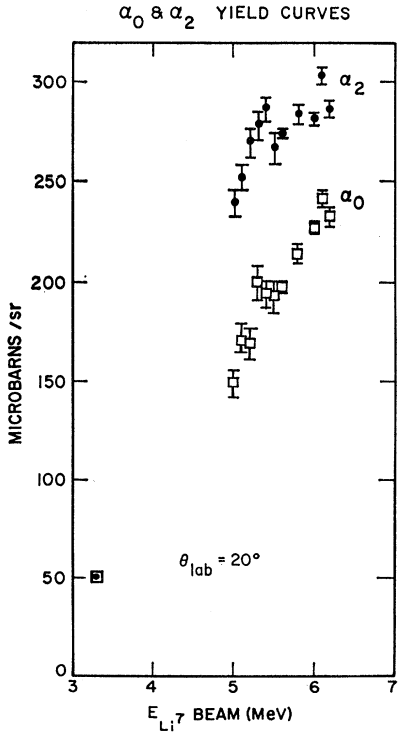

FIG. 10. α_0 yield curve and α_2 yield curve.

TABLE I. Absolute total cross sections (mb).

Li^7 lab energy	Protons C^{15}		Deuterons C^{14}						Tritons C^{13}			α's B^{12}			
	P_0	p_1	d_0	d_1	$d_{2,3}$	$d_{4,5}$	d_6	d_7	t_0	t_1	$t_{2,3}$	α_0	α_1	α_2	$\alpha_{3,4}$
5.60	0.218 ±0.032	0.822 ±0.066	0.542 ±0.042	1.74 ±0.09	3.75 ±0.15	2.88 ±0.13	2.50 ±0.10	1.96 ±0.20	1.56 ±0.07	1.51 ±0.08	6.22 ±0.22	2.49 ±0.26	3.38 ±0.24	3.45 ±0.22	3.46 ±0.17
5.80	0.248 ±0.027	0.909 ±0.074	0.551 ±0.041	1.55 ±0.08	3.58 ±0.15	2.69 ±0.13	2.35 ±0.11	1.84 ±0.20	1.51 ±0.08	1.28 ±0.06	5.94 ±0.23	2.52 ±0.27	3.41 ±0.24	3.82 ±0.25	3.67 ±0.23
6.00	0.287 ±0.060	0.891 ±0.263	0.566 ±0.054	1.52 ±0.11	3.56 ±0.23	2.92 ±0.22	2.41 ±0.17	1.88 ±0.25	1.59 ±0.12	1.30 ±0.10	6.22 ±0.38	2.76 ±0.33	3.59 ±0.32	3.76 ±0.34	3.87 ±0.33
6.20	0.271 0.040	0.929 0.103	0.569 ±0.034	1.51 ±0.06	3.68 ±0.09	2.78 ±0.08	2.33 ±0.07	1.86 ±0.20	1.58 ±0.06	1.30 ±0.05	6.17 ±0.11	2.79 ±0.29	3.82 ±0.22	4.42 ±0.27	4.73 ±0.22

TABLE II. $\sigma(0°–90°)$ Partial total cross sections (mb).

Li^7 lab energy	Protons C^{15}		Deuterons C^{14}						Tritons C^{13}				α's B^{12}			
	p_0	P_1	d_0	d_1	$d_{2,3}$	$d_{4,5}$	d_6	d_7	t_0	t_1	$t_{2,3}$	t_4	α_0	α_1	α_2	$\alpha_{3,4}$
5.60	0.097 ±0.013	0.384 ±0.051	0.231 ±0.023	0.794 ±0.038	1.85 ±0.06	1.49 ±0.05	1.31 ±0.05	0.782 ±0.044	0.820 ±0.038	0.666 ±0.035	3.09 ±0.08	1.41 ±0.37	0.997 ±0.178	1.79 ±0.20	1.46 ±0.10	1.24 ±0.08
5.80	0.103 ±0.016	0.446 ±0.069	0.243 ±0.034	0.688 ±0.037	1.73 ±0.07	1.38 ±0.06	1.15 ±0.06	0.877 ±0.044	0.829 ±0.045	0.548 ±0.032	3.03 ±0.15	1.42 ±0.34	1.04 ±0.18	1.70 ±0.20	1.46 ±0.14	1.28 ±0.14
6.00	0.118 ±0.041	0.439 ±0.261	0.280 ±0.048	0.715 ±0.048	1.80 ±0.22	1.60 ±0.21	1.25 ±0.16	0.970 ±0.132	0.970 ±0.116	0.643 ±0.092	3.45 ±0.37	1.50 ±0.37	1.24 ±0.27	1.90 ±0.30	1.58 ±0.29	1.56 ±0.30
6.20	0.108 ±0.014	0.428 ±0.101	0.267 ±0.023	0.695 ±0.033	1.82 ±0.05	1.47 ±0.05	1.15 ±0.04	0.970 ±0.040	0.884 ±0.037	0.542 ±0.031	3.32 ±0.07	1.57 ±0.39	1.14 ±0.20	1.79 ±0.19	1.63 ±0.12	1.52 ±0.16

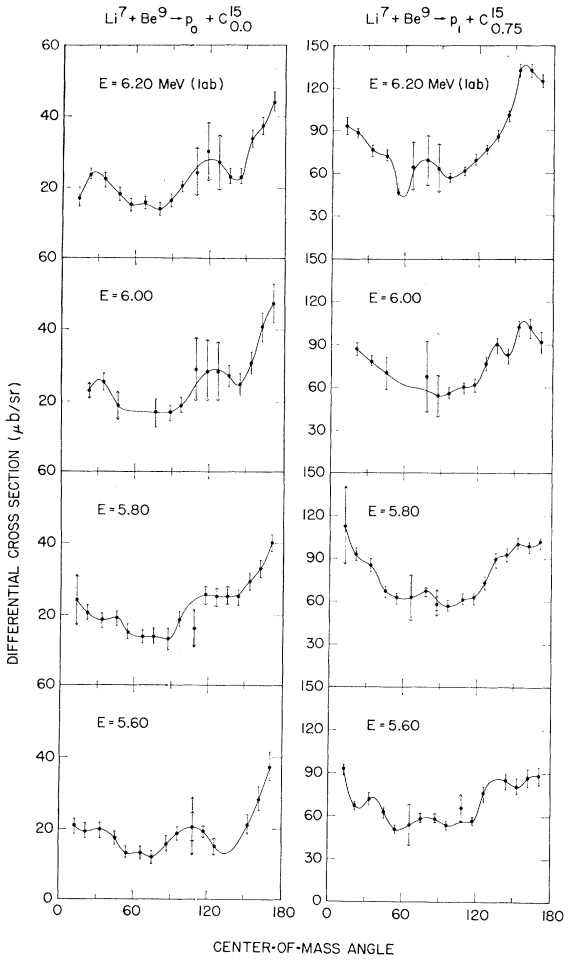

FIG. 11. $d\sigma/d\Omega$ for $Be^9+Li^7\rightarrow p_0+C_0^{15}$ and $Be^9+Li^7\rightarrow p_1+C^{15}{}_{0.75}$.

kinematic analysis of the proton groups at all of the angles investigated yielded energy values for the C^{15} states which agreed with those in the Lauritsen and Ajzenberg-Selove summary,[4] within the accuracy of the experimental results. Definite evidence was obtained for all of the states listed in that summary except the 2.48- and 8.00-MeV states, for which the evidence remains uncertain.

Each of the angular distributions shown in Figs. 11–18 was extrapolated to 0° and 180° and the total cross section for the particular reaction at the particular bombarding energy obtained by a trapezoidal numerical integration. These total cross sections are given in Table I. Though the t_4 group could not be followed over the whole angular range, we were able to follow it part way. The resulting partial angular distribution is given in Fig. 16, and the value of $d\sigma/d\Omega$ integrated from 0° to 90° is given in Table II and in Fig. 21.

The relative accuracy of these total cross section values is limited by the following factors: the accuracy of the individual points in the corresponding angular distributions, the extrapolation of the angular distributions to 0° and 180°, the trapezoidal numerical-integration techniques used (negligible effect here), the accuracy of the normalization to the α_0 yield curve, and the accuracy of that curve. The absolute value of a cross section is also dependent upon the accuracy of our absolute cross section determination in terms of the Coulomb scattering cross section. Our estimate of the errors due to all of these effects except this last, i.e., the relative accuracy of the total cross-section values, is represented by the error bars placed on the points in Figs. 19–22 and are given in Tables I and II.

Two types of comparison between theory and experimental results were made. A comparison was made of the total cross section with the so-called $(2J+1)$ rule. Agreement with such a rule is expected if the reaction goes via a statistical compound-nucleus mechanism and is also expected in some direct-reaction cases.[6,7] No

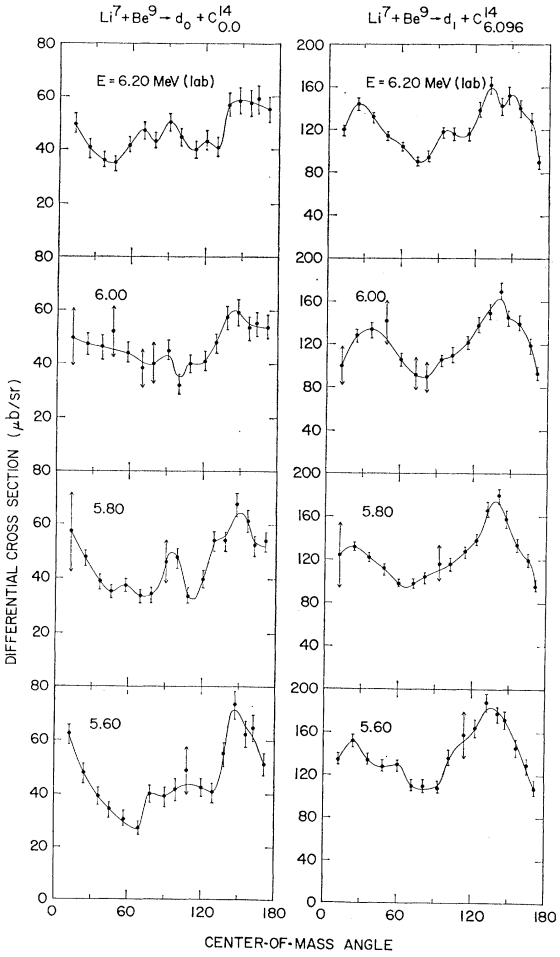

FIG. 12. $d\sigma/d\Omega$ for $Be^9+Li^7\rightarrow d_0+C_0^{14}$ and $Be^9+Li^7\rightarrow d_1+C^{14}{}_{6.10}$.

[6] N. Macdonald, Nucl. Phys. **33**, 110 (1962).
[7] S. Butler, *Nuclear Stripping Reactions* (Wiley-Interscience, Inc., New York, 1957), Chap. 12.

correction has been made for the variation of the cross section due to the energy and angular momentum dependence of the penetrability factor, which one should expect if the mechanism involves a statistical compound nucleus.[6] The results of the comparison are shown in the left sides of Figs. 19–22. Cross sections for unresolved states are plotted at

$$\sum_i (2J_i+1).$$

The values and error ranges shown are those given in Table I. Error bars are not indicated when the size of a point on the plot extends over the range of the error assigned. The points are plotted for the spin values shown in Fig. 1 except for the points corresponding to $Be^9(Li^7, d_7)C^{14}_{8.32}$ and $Be^9(Li^7, \alpha_{3,4})B^{12}_{2.62,2.72}$, where the spins of the final states are not known exactly. These points are discussed further below.

The total cross sections are seen to fit the $(2J+1)$ rule quite well for all four types of particles. The fit is especially good if one recalls that the effect of the penetrability correction would be to raise those points

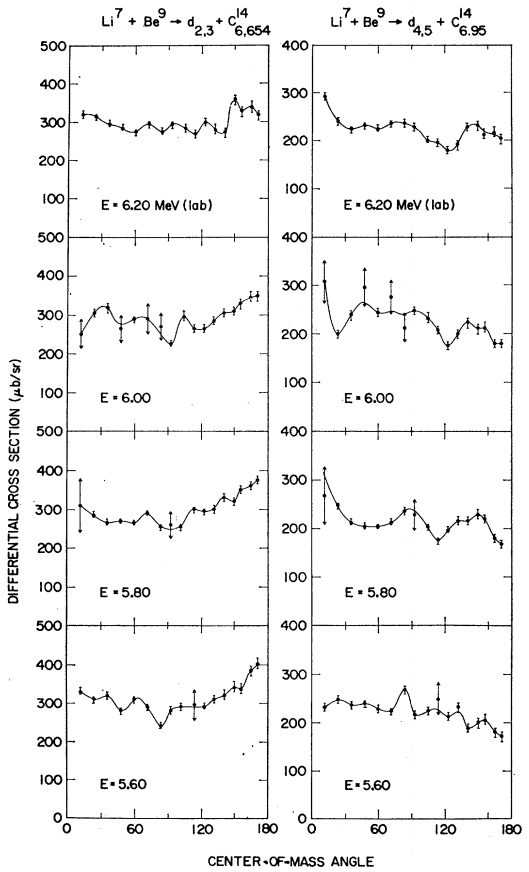

FIG. 13. $d\sigma/d\Omega$ for $Be^9+Li^7 \rightarrow d_{2,3}+C^{14}_{6.58,6.72}$ and $Be^9+Li^7 \rightarrow d_{4,5}+C^{14}_{6.89,7.01}$.

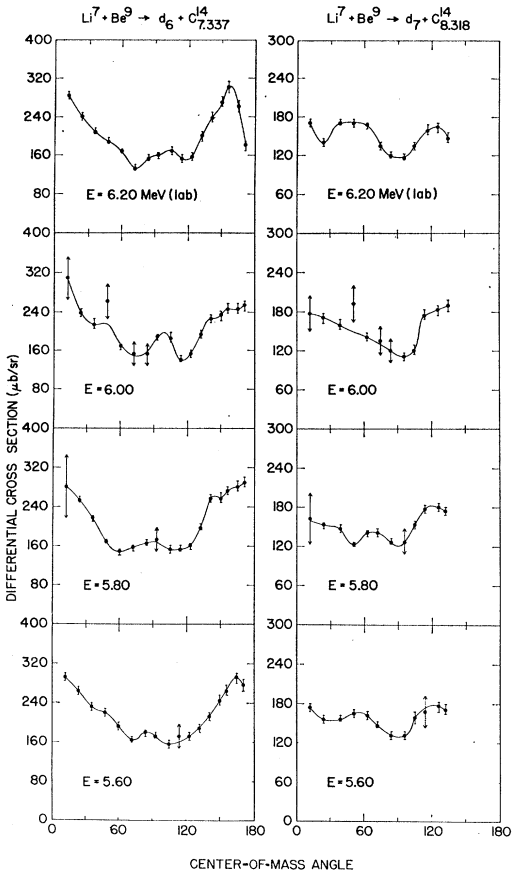

FIG. 14. $d\sigma/d\Omega$ for $Be^9+Li^7 \rightarrow d_6+C^{14}_{7.34}$ and $Be^9+Li^7 \rightarrow d_7+C^{14}_{8.32}$.

corresponding to the higher excited states and higher angular momenta and that this effect would be greater for the outgoing particles with higher Z, the α's.

It is surprising to find that the cross sections for all particle types fit the $(2J+1)$ rule so well. We plotted the cross section integrated from 0° to 90° as a function of $2J+1$ (these are the values given in Table II) and, as shown in the right sides of Figs. 19–22, these also fit the $(2J+1)$ rule quite well. If the reactions go via a compound mechanism, the angular distributions should by symmetric about 90° in the c.m. and the $\sigma(0°–90°)$ should, of course, fit the $(2J+1)$ rule as well as the $\sigma(0°–180°)$. But inspection of the angular distributions which we have obtained does not reveal such symmetry being the universal rule. If the reactions go via a direct-reaction mechanism, the modes would be stripping and knockout and probably only one of these, except perhaps in the case of the triton and α reactions. It is in the expressions for these two modes of direct reaction that the factor $2J+1$ does appear. The resulting $2J+1$ dependence of the total cross sections could be wiped out through interference effects between the two modes, if they both occur, or by fluctuations in the reduced

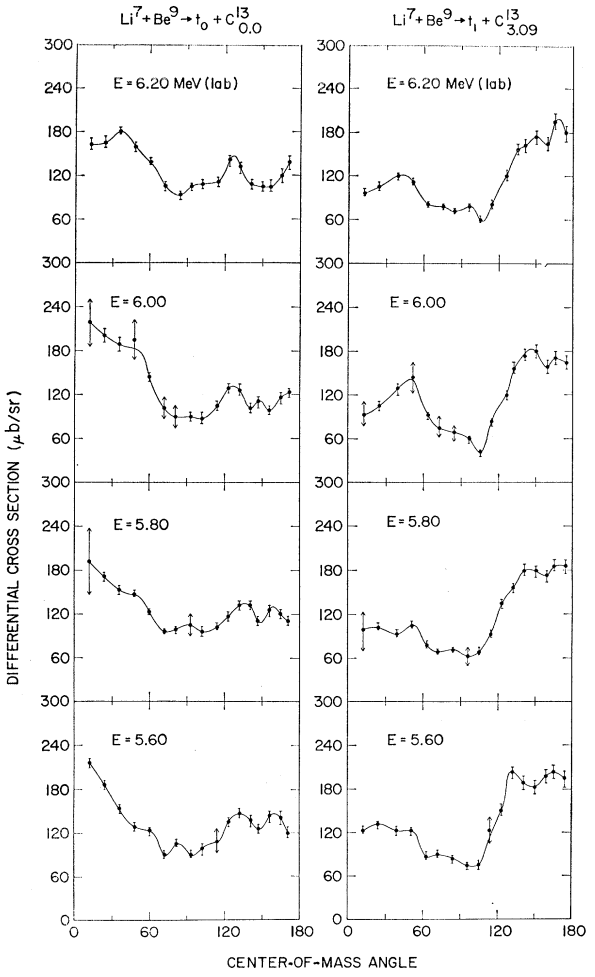

FIG. 15. $d\sigma/d\Omega$ for $Be^9+Li^7 \rightarrow t_0+C_0^{13}$ and $Be^9+Li^7 \rightarrow t_1+C^{13}_{3.09}$.

width from state to state of the final product nucleus. As noted, only one of the direct reaction modes is likely except in the case of the triton and α reactions, and the interference of the two modes would appear to be important enough to remove the $2J+1$ dependence of σ in these cases if not in the proton and deuteron reactions. One would expect the reduced width to be roughly constant if the final states had the same parentage. But, clearly, ours do not. The C^{15} states populated by the proton-producing reactions studied are supposedly two different single-particle states. In the case of each of the other types of reactions, leading to C^{14} or C^{13} or B^{12}, we have final states which have different parity and thus ones which certainly cannot have the same parentage. And, with the possible exception of the B^{12} states, even those states with the same parity are not considered to have the same parentage.

We thus remain somewhat puzzled by the fact that the cross sections for *all* the reactions obey the $(2J+1)$ rule so well, regardless of whether their angular distribution shows symmetry about 90° or not.

Returning to consideration of the two states for which exact spins had not previously been assigned, the J^π of the 8.32-MeV state of C^{14} has been assigned[4] values of $(1, 2)^+$. Glover and Jones[8] have chosen the 2^+ value on the basis of the $C^{13}(d, p)C^{14}_{8.32}$ angular distribution, and the 2^+ value would be preferred on the basis of the work of Warburton and Pinkston[9] on the N^{14} analog levels. Cohn, Bair, and Willard,[10] on the other hand, had concluded that the J^π was 1^+ on the basis of the neutron cross section for C^{13}. For the $(2J+1)$ rule comparison, Fig. 20, we have plotted the

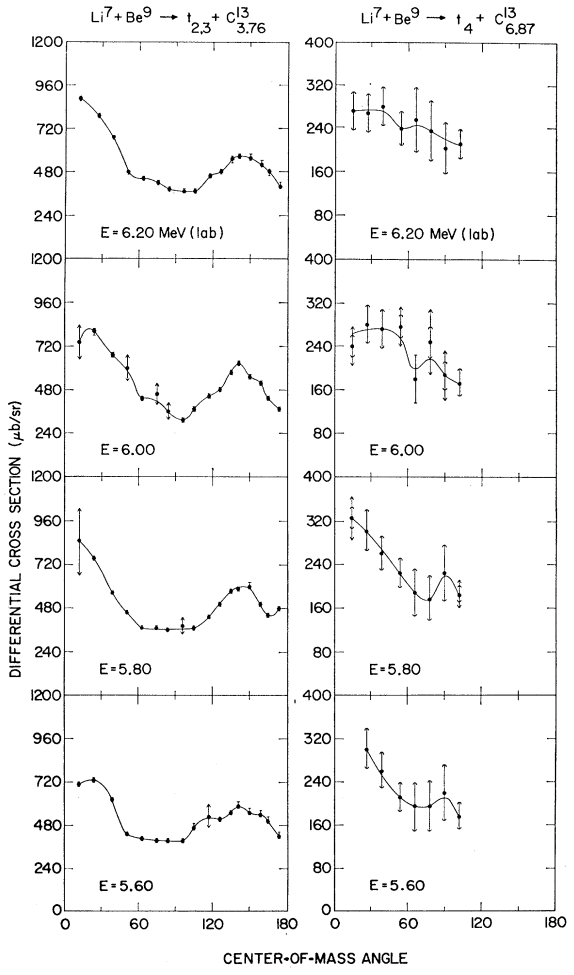

FIG. 16. $d\sigma/d\Omega$ for $Be^9+Li^7 \rightarrow t_{2,3}+C^{13}_{3.68,3.85}$ and $Be^9+Li^7 \rightarrow t_4+C^{13}_{6.87}$.

[8] R. N. Glover and A. D. W. Jones, Nucl. Phys. **84**, 673 (1966).
[9] E. K. Warburton and W. T. Pinkston, Phys. Rev. **118**, 733 (1960).
[10] H. O. Cohn, J. K. Bair, and H. B. Willard, Phys. Rev. **122**, 534 (1961).

cross sections for the $Be^9(Li^7, d_7)C^{14}_{8.32}$ reaction at each of these values, $J=1$ and $J=2$. The $J=2$ value puts the point below the line, the $J=1$ value above. If the point should lie on the line, we would prefer the 2^+ assignment, accounting for the position of the point below the line by the energy dependence of the penetrability factor. But either value would be consistent with the data.

The J^π of the 2.72-MeV level of B^{12} has a previously assigned[4,11] value of $(\leq 3)^+$. The work of Gallman *et al.*[12] and that of Segel *et al.*[13] give some preference to the 0^+ assignment. The cross section for the $Be^9(Li^7, \alpha_{3,4})B^{12}_{2.62,2.72}$ reaction has been plotted in Fig. 22 at a point appropriate to an assignment of $J=0$ as well as at a point appropriate to an assignment of $J=1$ to the 2.72-MeV level of B^{12}. An assignment of a larger spin value would make the point fall well outside the region indicated by the $(2J+1)$ behavior of all the other α groups. Again, either assignment, $J=0$ or $J=1$, would be consistent with our data, with some preference for the $J=0$ assignment.

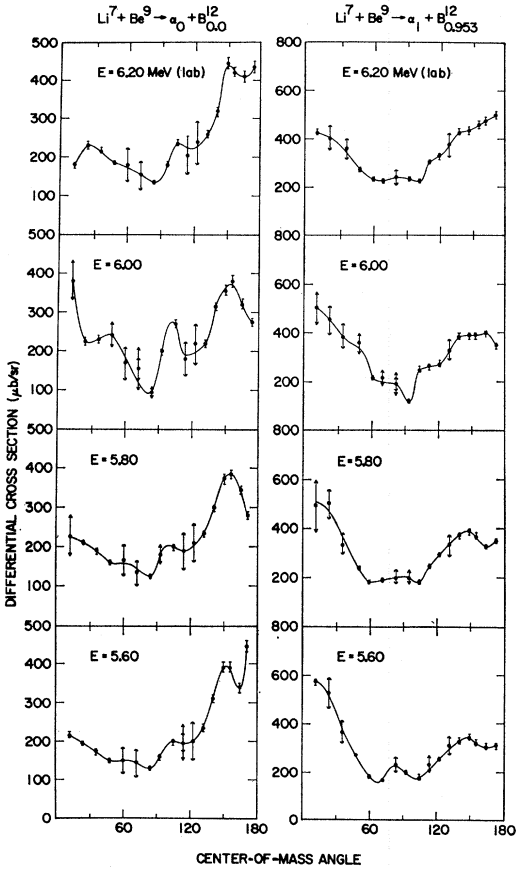

FIG. 17. $d\sigma/d\Omega$ for $Be^9+Li^7 \rightarrow \alpha_0+B_0^{12}$ and $Be^9+Li^7 \rightarrow \alpha_1+B^{12}_{0.95}$.

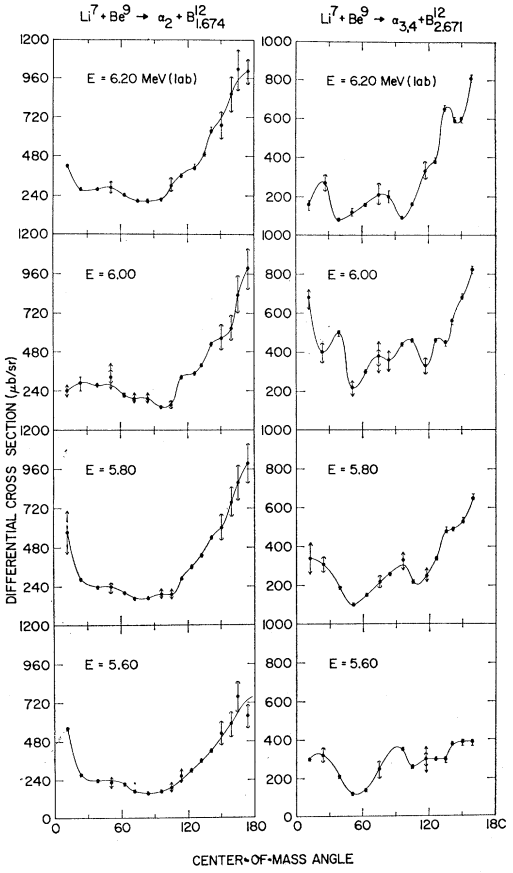

FIG. 18. $d\sigma/d\Omega$ for $Be^9+Li^7 \rightarrow \alpha_2+B^{12}_{1.67}$ and $Be^9+Li^7 \rightarrow \alpha_{3,4}+B^{12}_{2.62,2.72}$.

In addition to the comparison of the total cross section values with the $(2J+1)$ rule, the angular distributions of the t_0 and t_1 groups at each of the four energies were compared with the predictions of a two-mode direct-reaction-mechanism model. The reaction $C^{13}+t \rightarrow Li^7+Be^9$ was considered to go by pickup and/or heavy-particle stripping, the latter an exchange mechanism. Proton, deuteron, and α-particle reactions were not tried here because of the large number of l and j values possible.

The basic form of the theoretical treatment used is that of Fulton and Owens[14] and Warsh and Edwards.[15] A plane-wave approximation is made and the structure of the incident particle, the triton in our case, is neglected. The differential cross section for the two-

[11] F. A. Ajzenberg-Selove and T. Lauritsen, Nucl. Phys. **A114**, 1 (1968).
[12] A. Gallman, F. Hibou, P. Fintz, P. E. Hodgson, and E. K. Warburton, Phys. Rev. **138**, 560 (1965).
[13] R. E. Segel, S. S. Hanna, and R. G. Allas, Phys. Rev. **139**, 818 (1965).
[14] R. Fulton and G. E. Owen, Phys. Rev. **108**, 789 (1957).
[15] S. Edwards, Notes by L. L. Warsh, Tandem Van de Graaff Accelerator Laboratory, Florida State University, 1961 (unpublished).

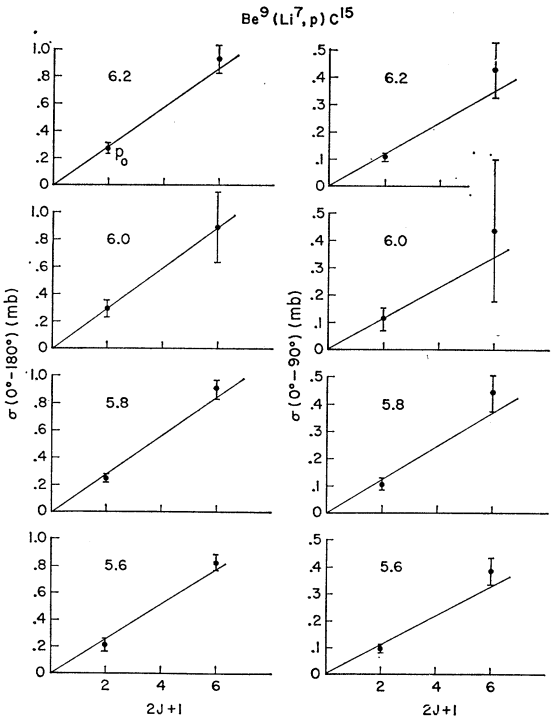

FIG. 19. σ versus $2J+1$ for protons.

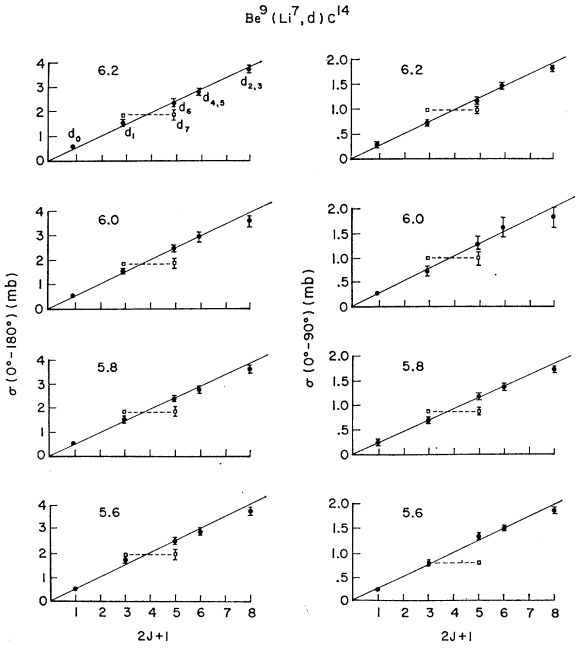

FIG. 20. σ versus $2J+1$ for deuterons.

mode reaction case can be written as

$$d\sigma/d\Omega \propto (k_{\mathrm{Li}^7}/k_t)[S_P A_P^2 + C^2 S_E A_E^2 - 2f(\theta) C A_P A_E],$$

the first term resulting from the pickup mode, the second from the exchange or heavy-particle stripping mode, and the third from the interference between the pickup and exchange modes. The k_{Li^7} and k_t are the wave vectors for the Li^7 and the triton in the c.m. system, A_P and A_E are amplitude factors containing the energy and momentum dependence of the pickup and exchange modes, and C is the ratio of the amplitude of

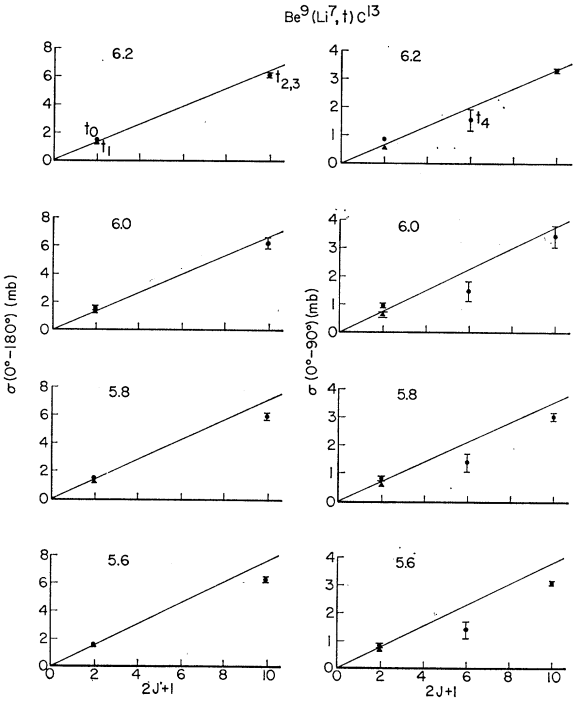

FIG. 21. σ versus $2J+1$ for tritons.

the two modes. The values of the factors S_P, S_E, and $f(\theta)$ result from the coupling of the angular momenta involved in the various modes. In determining the values of these factors, we have used the known J^π values of the systems involved and conservation of angular momentum and parity. In both the t_0 and t_1 cases studied, the value of S_P was a constant and we have factored it out and written $d\sigma/d\Omega$ as

$$d\sigma/d\Omega = N(E)\,(A_P^2 + S'_E C^2 A_E^2 - 2f'(\theta) A_P A_E),$$

where $N(E)$ is the "normalization factor" between theory and experiment.

Each of the amplitude functions A_P and A_E can be

TABLE III. Values of parameters for two-mode fits.

Reaction	E_{Li^7}(lab) (MeV)	r_1 (F)	a_1 (F)	r_2 (F)	a_2 (F)	Normalization C	factor (10^{11})
$Be^9(Li^7, t_0)C_0^{13}$	6.20	2.52	1.41	2.91	1.92	2349	8.48
	6.00	2.54	1.53	2.96	1.94	2479	9.90
	5.80	2.57	1.53	2.94	1.86	2159	9.82
	5.60	2.60	1.48	2.97	1.90	2539	9.42
$Be^9(Li^7, t_1)C^{13}_{3.09}$	6.20	2.47	1.11	3.46	1.76	5861	1.29
	6.00	2.50	1.10	3.50	1.80	6400	1.28
	5.80	2.47	1.22	3.50	1.76	6751	1.09
	5.60	2.47	1.33	3.53	1.76	6624	1.48

expressed in terms of the bombarding energy E, the reaction angle θ, and two cutoff radii corresponding to the lower limits of the Butler integrals for the pickup process and analogous integrals for the exchange process. The symbols used and the interactions with which the cutoff radii are associated are as follows for the $C^{13}(t, Li^7)Be^9$ reaction:

Pickup: r_1 for t and α in outgoing Li^7,

a_1 for α and Be^9 in target C^{13};

Exchange: r_2 for t and Li^6 core in residual Be^9,

a_2 for Li^7 and Li^6 core in target C^{13}.

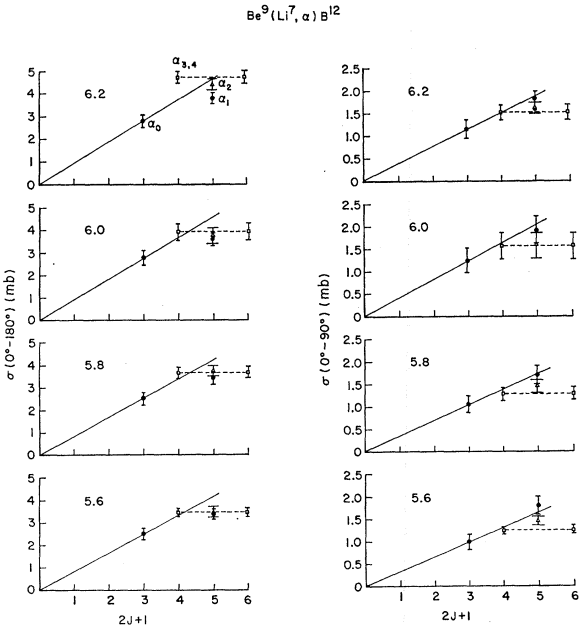

FIG. 22. σ versus $2J+1$ for α particles.

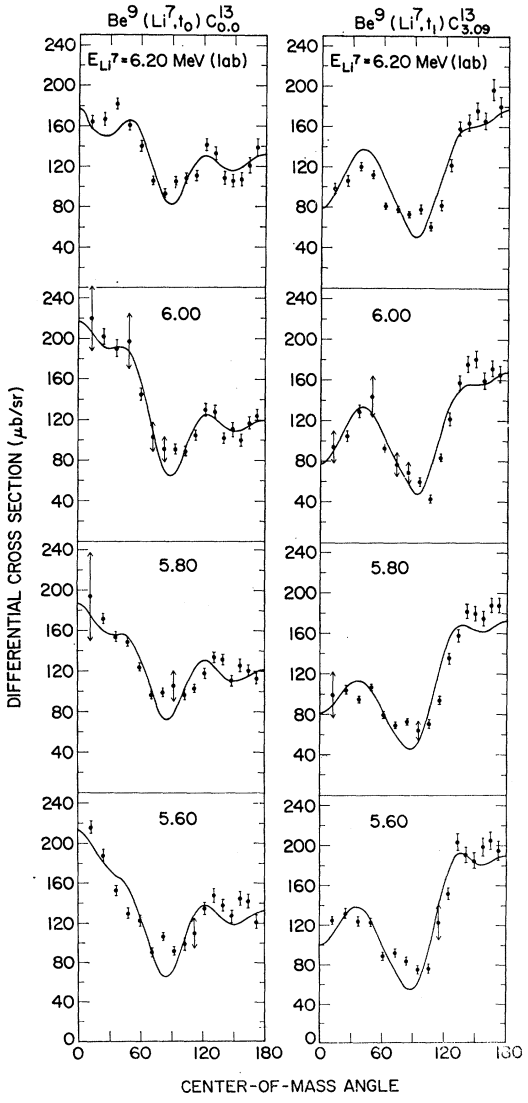

FIG. 23. Results of plane-wave, two-mode, direct-reaction theory fits to angular distributions. The values of the parameters for the fits are given in Table III.

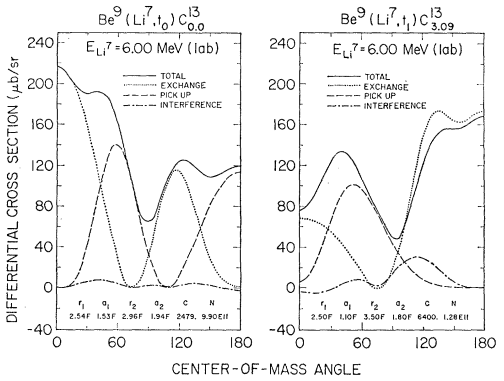

FIG. 24. Illustration of the contribution of pick up (– – –), exchange (• • •), and interference (–•–) terms to the total (——) cross section.

The angular distribution for the $Be^9(Li^7, t_0)C^{13}_{0.0}$ and the $Be^9(Li^7, t_1)C^{13}_{3.09}$ reactions were fit at each of the four bombarding energies studied experimentally, using the four cutoff radii and C as parameters. The full angular range of experimental data was used. Various criteria for normalization and for goodness of fit were employed in the search programs, and over 100 different sets of starting values for the parameters were used in the attempt to find the most satisfactory fit to an angular distribution. Programs which simply stepped through various values of the parameters and plotted out the resulting angular distributions for our inspection were used in addition to search programs employing some fixed criteria for fit and normalization. Satisfactory sets of parameters were considered to be ones which not only gave good fits to each of the angular distributions, but which also, for a given reaction, were constant or at most varied slowly and smoothly with bombarding energy.

The "best fits" to our angular distributions are shown in Fig. 23. The values of the parameters and normalization factor for these fits are given in Table III. In Fig. 24 we have plotted the contributions of the various terms in the theoretical expression for the cross section, pickup, heavy-particle stripping, and interference for the $E_{Li^7}=6.0$ MeV case for each of the two reactions, in order to indicate the characteristics in the angular distributions due to each term.

The fits obtained are quite reasonable and the value of the parameters certainly satisfy the criterion that they be constants or slowly varying functions of energy for a given reaction. The parameter C can sometimes be a rather insensitive determinant of a good fit, interplaying somewhat with the normalization factor when one of the reaction amplitudes is small relative to the other amplitude. But even it behaves. We have made no test of the absolute magnitude of the normalization factor since the wave functions used in the theoretical expression were not normalized. The variation of N with bombarding energy is reasonable, however.

The fits shown are the best obtained. Other acceptable fits at other sets of values of the parameters could be obtained for one or two of the angular distributions but no other set was found which fit the angular distributions for a given reaction at all of the energies. In addition, the relative values of the parameters for the two different reactions is acceptable. We suspect that there may be another set of larger radii which would give good fits but have been unable to locate a satisfactory set.

Because of the $(2J+1)$ dependence of the cross section discussed above, we tried subtracting an isotropic background or a $\cos^2\theta$ dependent background from the data and fitting the remainder—even though this in effect added still another parameter to the number available. However, we did not find a set of parameters which gave good fits to all of the distributions for a given reaction, and certainly not ones which made sense when compared with the values for the other reaction.

ACKNOWLEDGMENTS

We should like to express our appreciation to Professor R. R. Carlson for the original version of some of the on-line computer programs used in the experimental work, and to Geoffrey Hartnell for his efforts in providing us with a Van de Graaff in working order.